






## Innovative fluorescent nanocomposite eutectogels: Design and characterization towards biosensing applications

Yolanda Alacid<sup>a,b,1</sup> , Raúl Martínez-Baquero<sup>a,b,1</sup> , Rocío Esquembre<sup>a</sup>, Francisco Montilla<sup>b</sup> ,  
María José Martínez-Tomé<sup>a,\*</sup>, C. Reyes Mateo<sup>a,\*</sup>

<sup>a</sup> Instituto de Investigación, Desarrollo e Innovación en Biotecnología Sanitaria de Elche (IDI<sup>BE</sup>), Universidad Miguel Hernández, Avenida de la Universidad s/n, 03202 Elche, Alicante, Spain

<sup>b</sup> Departamento de Química Física and Instituto Universitario de Materiales de Alicante (IUMA), Universidad de Alicante, Carretera San Vicente s/n, 03690 Alicante, Spain

### ARTICLE INFO

#### Keywords:

Fluorescent eutectogels  
Nanoparticles  
Conjugated polymers  
Deep eutectic solvents  
Eutectozymes  
Alkaline phosphatase

### ABSTRACT

Recent advancements in materials science have led to the creation of innovative gel formulations like eutectogels, which exploit the distinctive characteristics of deep eutectic solvents (DES) to enhance the functionality and versatility of traditional gel systems. By incorporating fluorescent nanoparticles, eutectogels gain luminescent properties, significantly increasing their performance. In this study, we have developed and characterized a novel nanocomposite eutectogel by integrating conjugated polymer-based nanoparticles (CPNs) with varying emission bands, derived from either polyfluorene or poly(phenylenevinylene). Before synthesizing the fluorescent eutectogels, it was confirmed that the nanoparticles maintained the same fluorescent properties in both DES and aqueous solution. The results show that the incorporation of CPNs inside the eutectogels provides fluorescent materials with good properties in terms of integrity, thermal stability, homogeneity and reproducibility allowing their preservation during weeks. The fluorescent nanocomposite eutectogels were tested as sensing platforms by immobilizing enzymes. In particular, the capability of these materials to act as fluorescent biosensors for detecting hydrolase activity was successfully demonstrated, with alkaline phosphatase entrapped in the nanocomposite eutectogel serving as the model enzyme. This finding is one of the first demonstrations of the functioning of an enzyme in an eutectogel.

### 1. Introduction

Polymeric gels are an important class of soft matter systems composed of a highly dispersed liquid phase and one or more solid continuous phases. The continuous phase generates a cross-linked 3D network structure, through covalent or non-covalent bonds, inside which are the liquid molecules. The result is a viscoelastic material, similar to a solid, but highly deformable [1]. The degree of crosslinking and the functional groups of the polymer chains influence properties such as stiffness, swelling ratio, elasticity, degree of transparency and processability of the material. Depending on the nature of the liquid phase, gels can be classified into organogels (organic solvent) and hydrogels (water), although the development of neoteric solvents has expanded this classification, also including ionogels (ionic liquids), and more recently eutectogels (EGs), when the liquid phase is a deep eutectic

solvent (DES) [2–4].

DES, typically consisting of mixtures of hydrogen bond donors (HBDs) and hydrogen bond acceptors (HBAs) in various molar ratios, have a number of unique properties, such as low volatility, thermal stability, biodegradability and moderate to very low toxicity, depending on the starting ingredients, as well as maximum atomic economy, making them a sustainable alternative to traditional solvents [5–7]. The HBAs most commonly used in DES formulation are quaternary ammonium salts, in particular choline chloride (ChCl) due to its low toxicity, low cost and biodegradability, while HBDs typically include an organic molecular component such as an amide, carboxylic acid, or polyol (urea, oxalic acid, glycerol, ethylene glycol (EtG)), etc [8]. The immobilization of DES in polymeric matrices to produce EGs offers new opportunities in the field of novel materials, since compared to gels prepared using other solvents, they possess excellent elasticity, ionic conductivity, non-

\* Corresponding authors.

E-mail addresses: [mj.martinez@umh.es](mailto:mj.martinez@umh.es) (M.J. Martínez-Tomé), [rmateo@umh.es](mailto:rmateo@umh.es) (C.R. Mateo).

<sup>1</sup> Equal authorship.

volatile nature that confers higher thermal stability, ability to solubilize hydrophilic and hydrophobic agents and adhesion properties. In addition, their properties can be finely tuned by selecting different DES components and varying their ratios, allowing for greater customization of the gel characteristics. As a consequence of such properties, these newly emerging materials are attracting great interest in the biomedical field, as well as offering new perspectives as dynamic functional platforms in both water-free and water-containing environments [9–12].

The most common and simple method for making EGs is to immerse a previously prepared hydrogel in a DES for solvent replacement. Another approach is the polymerization of the gel network in DES directly, by dissolving the monomers (acrylic acid, methacrylic acid,...) before initiating radical polymerization. Also, polymerizable monomer units can act as HBAs or HBDs to form DES, and then directly polymerize inside the DES to form the eutectogel [12,13]. Finally, EGs can be obtained by the addition of low molecular weight organic gelators that self-assemble into a nanoscale network as a result of non-covalent intermolecular interactions [14]. Regardless of the preparation method of the eutectogel, its properties can be modulated by incorporating nanomaterials inside it, through chemical or physical crosslinking. As with hydrogels, this strategy results in nanocomposites with improved performance as a result of the synergistic effect between the two components. Although recent research in these type of materials is still in its infancy, nanocomposite EGs have already been described that include, among others, nanocrystals, metallic and polymer nanoparticles, or carbon nanotubes in their composition. Thus, Bianchi et al. recently have reported the synergistic combination of drug nanocrystals and a eutectic mixture supported into a gelatin matrix to obtain stretchable and adhesive eutectogels for long-acting mucosal delivery [10]. A very recent work describes the incorporation of silver nanoparticles and phosphorus nanoflakes into a ChCl:glycerol-cellulose eutectogel, thus endowing the material with antibacterial properties [15]. In another recent paper, a novel magnetic eutectogel which includes a polymeric deep eutectic solvent, multiwall carbon nanotubes, and superparamagnetic polyvinylpyrrolidone coated-Fe<sub>3</sub>O<sub>4</sub> nanocrystals incorporated in alginate gel, has been prepared and used as sorbent in the microextraction of pesticides [16]. Also, lignin nanoparticles have been uniformly dispersed in a ChCl:EtG-PVA gelatin eutectogel increasing its mechanical properties, leading to materials with potential use as wearable flexible strain sensors [17].

The incorporation of fluorescent nanoparticles in EGs endow these materials with luminescent properties that can be exploited, besides other applications, for the development of optical sensors and as bio-imaging tools. However, to the best of our knowledge, these nanocomposite materials have not been explored in the literature, although some studies on fluorescent eutectogels are available. Thus, recently, a reversible fluorescent eutectogel with high transparency, adhesiveness and self-healing has been developed, but it uses anthracene molecules as luminescent units, instead of nanoparticles [18]. In addition, Criado-González et al. have just developed a fluorescent eutectogel by combining a low molecular weight fluorescent gelator derived from glutamic acid with poly(3,4-ethylenedioxythiophene) and ChCl-based DES, to obtain mixed ionic/electronic conductive composites for bio-imaging applications [11].

Some of the fluorescent nanomaterials that can be incorporated into EGs include: semiconductor quantum dots (SQDs), carbon dots (CQDs), graphene quantum dots (GQDs) and conjugated polymers-based nanoparticles (CPNs). SQDs have high light emission and can easily adjust their optical properties through changes in size and composition, but present toxicity issues due to heavy metals [19]. CQDs and GQDs have higher compatibility with living organisms and lower toxicity. Although they generally show lower fluorescence efficiency than SQDs, this limitation can be improved with surface passivation or functionalization [20–23]. Finally, CPNs exhibit good biocompatibility, excellent photostability and high quantum efficiency, and unlike CQDs, their fluorescence emission can be fine-tuned across a wide spectral range by

appropriate design of the polymer molecular backbone [24,25].

In addition to incorporating nanomaterials into the EGs, another approach to increase its functionality is to include biological elements, such as enzymes. This new category of materials, denoted as eutecto-zymes, has been reported in two recent works in which authors describe the potential opportunities that this combination would offer, resulting in functional materials with unique properties which could show plain benefits compared to traditional hydrogels [9,26]. However, despite these potential advantages, to our knowledge no study has yet been conducted in which an enzyme has been incorporated into an eutectogel and its activity has been tested.

This work describes the synthesis and characterization of fluorescent nanocomposite EGs by the introduction of CPNs with different emission bands, made either from polyfluorene derivatives: poly[9,9-dioctylfluorenyl-2,7-diyl] (PFO) and poly[(9,9-di-n-octylfluorenyl-2,7-diyl)-alt-(1,4-benzo-{2,1,3}-thiadiazole)] (F8BT) or with a poly(phenylenevinylene) derivative: poly[2-methoxy-5-(2'-ethylhexyloxy)-1,4-phenylenevinylene] (MEHPPV) (Scheme 1a). EGs were prepared via a simple and rapid protocol based in previous works through UV-induced *in situ* radical polymerization of suitable precursors in appropriate DES [27,28]. For the synthesis, the monomer 2-hydroxyethyl methacrylate (HEMA) was dissolved in a ChCl:EtG DES (1:2 M ratio) along with the crosslinker ethylene glycol dimethacrylate (EGDMA), the photoinitiator and the respective CPNs, obtaining fluorescent nanocomposite EGs with emission in the blue, yellow and red regions of the visible spectrum.

The fluorescent properties and stability of the different EGs were characterized and compared with those of nanoparticles in DES and water. In addition, their ability to be used as fluorescent biosensor was explored by incorporating the enzyme alkaline phosphatase (ALP) into the eutectogel. It is noteworthy that the immobilization of ALP in these materials constitutes a novelty since it is the first time that this type of enzyme is dissolved in DES and immobilized in an eutectogel, retaining its activity.

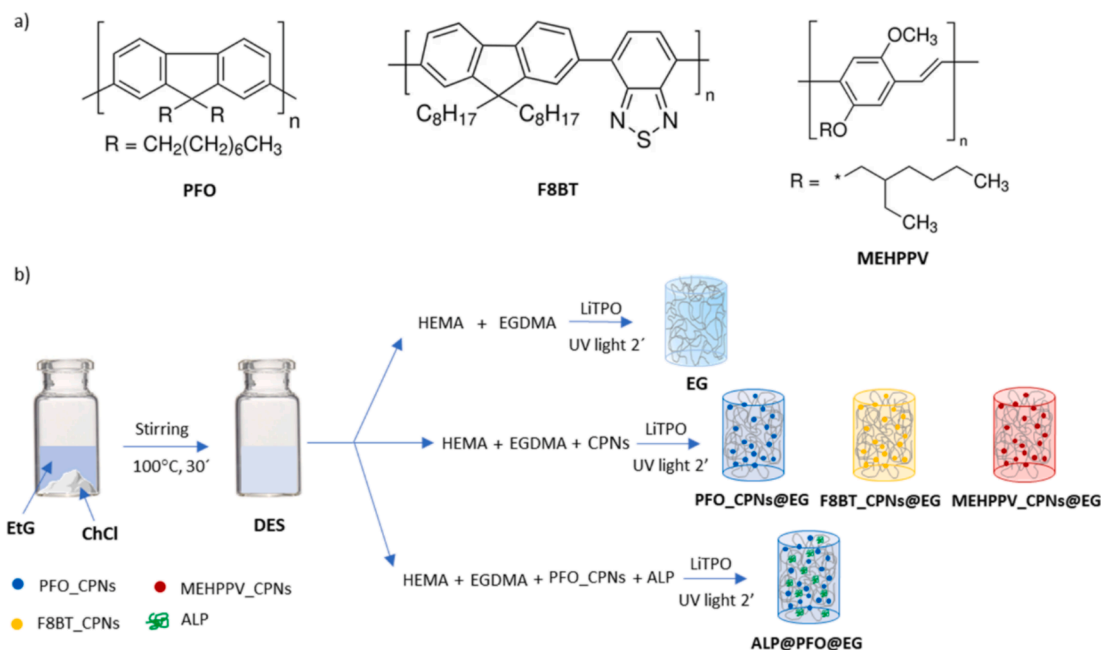
## 2. Materials and methods

### 2.1. Chemicals

2-Hydroxyethyl methacrylate (HEMA), ethylene glycol dimethacrylate (EGDMA), 2,4,6-trimethylbenzoylphenylphosphinate lithium salt (LiTPO), choline chloride (ChCl), alkaline phosphatase (ALP; EC 3.1.3.1; from bovine intestinal mucosa, lyophilized powder, 38 U/mg solid), *p*-nitrophenyl phosphate (PNPP), *p*-nitrophenol (PNP) and sodium dodecyl sulfate (SDS) were purchased from Sigma-Aldrich (Merck Life Science, Madrid, Spain). Ethylene glycol (EtG) (extra pure) was obtained from Scharlab (Spain). The conjugated polymers poly[9,9-dioctylfluorenyl-2,7-diyl] (PFO) and poly[(9,9-dioctylfluorenyl-2,7-diyl)-alt-co-(1,4-benzo-{2,1,3}-thiadiazole)] (F8BT) were sourced from American Dyes Source, Inc., while poly[2-methoxy-5-(2'-ethylhexyloxy)-1,4-phenylenevinylene] (MEHPPV) was acquired from Sigma-Aldrich. TRIS buffer (55 mM, pH 9) was prepared by dissolving TRIS base in Milli-Q water and adjusting the pH with hydrochloric acid. Milli-Q water was obtained using Milli-Q equipment (Millipore, Madrid, Spain). All other reagents used were of analytical grade and obtained from standard commercial suppliers.

### 2.2. Preparation of CPNs

Fluorescent nanoparticles were synthesized in an aqueous medium using the conjugated polymers PFO, F8BT and MEHPPV, following the miniemulsion method previously outlined by Pecher et al. [29] To achieve this, 5 mL of a 10 mg/mL conjugated polymer solution in toluene was combined with 10 mL of 55 mM TRIS buffer and 4 mg/mL SDS in water. The mixture was stirred for 1 h with a magnetic stirrer in a sealed vial. Next, the sample was subjected to ultrasonic treatment using a QSonica Q125 sonicator (QSonica, Newtown, CT, USA) at 125 W for



**Scheme 1.** Chemical structure of the conjugated polymers (CPs) PFO, F8BT, and MEHPPV (a). Scheme of eutectogels preparation and immobilization of fluorescent CPNs and ALP (b).

15 min, operating at 90 % amplitude, while keeping the vial immersed in an ice-water bath to prevent overheating and foam formation. The organic solvent was then evaporated by heating the mixture to 60 °C. The resulting solution was stored at 4 °C.

### 2.3. Preparation of DES

DES were prepared by combining ChCl and EtG in a 1:2 M ratio, followed by stirring at 100 °C for 30 min until a clear, homogeneous liquid was formed (Scheme 1b).

### 2.4. Preparation of eutectogels (EGs)

Eutectogels were prepared following the protocol described by Chen et al. [27], with slight modifications. In a vial, 600 µL of HEMA, 600 µL of the DES ChCl:2 EtG and 10 µL of EGDMA were mixed and stirred thoroughly. The photoinitiator LiTPO (2 mg) was then added under dark conditions and stirred until fully dissolved. The mixture was subsequently transferred into a 2 mL syringe, from which 1 mL was dispensed and exposed to UV light at 365 nm for 2 min to induce polymerization. Once polymerized, the tip of the syringe was cut and the eutectogel was demolded.

### 2.5. Preparation of nanocomposite EGs

To obtain nanocomposite eutectogels, CPNs were incorporated to the initial mixture prior to polymerization. This was done by adding 1 µL/mL of a 5 mg/mL nanoparticle stock solution to the HEMA-DES-EGDMA-LiTPO mixture. After UV irradiation, fluorescent eutectogels were produced, exhibiting blue (PFO\_CPNS@EG), yellow (F8BT\_CPNS@EG), and red (MEHPPV\_CPNS@EG) emissions (Scheme 1b).

### 2.6. Incorporation of ALP in PFO\_CPNS@EGs

Fluorescent eutectozymes were prepared by incorporation of the enzyme ALP into the PFO\_CPNS@EGs. For this purpose, lyophilized ALP powder was added to the PFO\_CPNS-HEMA-DES-EGDMA-LiTPO mixture to achieve a final concentration of 106.8 U/mL. The procedure was continued as in sections 2.4 and 2.5, placing the mixture under the UV

lamp and irradiating it for 2 min to induce polymerization. The obtained eutectogels, referred to as ALP@PFO@EGs, were stored in the refrigerator until activity tests were performed, using PNPP as substrate (Scheme 1b).

### 2.7. Particle size determination and zeta potential

The size and zeta potential of PFO, F8BT and MEHPPV CPNs were determined in water using dynamic light scattering (DLS) with a Malvern Zetasizer Nano-ZS instrument (Worcestershire, UK), which utilizes a 4 mW monochromatic helium–neon laser ( $\lambda = 633$  nm) as the light source. Size measurements were conducted at a scattering angle of 173° in disposable cuvettes, while zeta potential was measured using designated zeta potential cells. All measurements were performed in triplicate at 20 °C.

### 2.8. Fluorescence characterization of CPNs

Steady-state fluorescence measurements of CPNs in water, DES and immobilized in EGs were conducted in 10 × 10 mm quartz cuvettes using a PTI-QuantaMaster spectrofluorometer (PTI, Birmingham, NJ, USA) equipped with a Peltier cell. To obtain the emission spectra, samples were excited at wavelengths of 396 nm (PFO\_CPNS), 466 nm (F8BT\_CPNS) and 495 nm (MEHPPV\_CPNS), while for the excitation spectra the emission wavelength was fixed at 500, 600 and 660 nm, respectively. All fluorescence measurements were carried out at 20 °C, with the exception of the thermal stability study, for which spectra were recorded from 20 to 60 °C, with heating rates of 1 °C/minute. Background intensities were always checked and subtracted from the sample when it was necessary. All the samples were coloured, free of turbidity, and visually homogeneous.

Time-resolved fluorescence measurements were carried out by a high-performance fluorescence lifetime spectrometer FluoTime 300 (PicoQuant, Berlin, Germany), with time-correlated single-photon counting (TCSPC). Excitation sources used were picosecond pulsed diode lasers LDH-P-C-375, LDH-P-C-450, and LDH-P-C-520, with maximum excitation wavelengths of 373, 453 and 514 nm, respectively. Fluorescence intensity decays of CPNs in aqueous solutions, DES and eutectogels were recorded and analyzed with EasyTau software

(PicoQuant, Berlin, Germany) applying a tri-exponential decay model. The instrument response function was measured by using diluted Ludox® as scattering agent. The conditions applied to consider a satisfactory fit were a reduced  $\chi^2$ , close to 1, and random distributions of the weighted residuals. The intensity-weighted mean lifetimes were calculated from the recovered parameters of the fitting according to

$$\langle \tau \rangle = \frac{\sum a_i \tau_i^2}{\sum a_i \tau_i} \quad (1)$$

where  $\tau_i$  and  $a_i$  are the lifetimes and amplitudes, respectively, of the individual components.

## 2.9. Quenching studies

The effect of PNP on the fluorescence of CPNs was studied both in solution and inside the eutectogels. In the solution experiments the decrease in fluorescence intensity was analysed according to an expression based on Stern-Volmer equation:

$$\frac{I_0}{I} = 1 + K[Q] \quad (2)$$

where,  $I_0$  and  $I$  correspond to the fluorescence intensity of CPNs in absence and presence of PNP, respectively,  $[Q]$  is the concentration of PNP (the quenching agent), which was varied between 0 and 20  $\mu\text{M}$ , and  $K$  is a constant whose meaning depends on the nature of the quenching process and informs about the sensitivity of the nanoparticles to the presence of PNP, the higher the value of  $K$  the greater the capacity to detect its presence.

For the quenching experiments in fluorescent EGs, these were prepared using a disposable syringe, as detailed in Sections 2.4–2.5. Once removed from the syringe, the EGs showing a cylindrical shape with an average diameter of about 0.8 cm and a length of about 1.7 cm, were directly placed into the fluorescence cuvette without any prior manipulation or cutting. The initial fluorescence of the gels ( $I_0$ ) was measured, followed by the addition of 1 mL of a PNP solution at concentrations of 20, 50, or 100  $\mu\text{M}$ . The mixture was incubated for 20 min, after which the fluorescence spectrum was recorded. The emission intensity at the wavelength of the maximum peak was compared with that previously obtained in the absence of PNP. For each concentration, 6 replicates were made.

The possibility of inner filter effect (IFE) being responsible for the quenching caused by PNP was evaluated using the following equation [30,31]:

$$I_{cor} = I_{obs} \frac{A_T^x (1 - 10^{A_F^x})}{A_F^x (1 - 10^{A_T^x})} \frac{2.303A_T^m}{(1 - 10^{A_T^m})} \quad (3)$$

where  $I_{cor}$  and  $I_{obs}$  are the corrected and the measured fluorescence intensities, respectively,  $A_F^x$  and  $A_T^x$  represent the absorbance values of the samples in absence and presence of PNP, respectively, measured at the excitation wavelength and  $A_T^m$  is the absorbance of the sample measured at the emission wavelength.

The absorbance measurements were performed at room temperature with a UV-2700 spectrophotometer (Shimadzu, Tokyo, Japan). Measurements were taken using quartz cuvettes measuring  $10 \times 10$  mm.

## 2.10. Rheological measurements

The rheological measurements were conducted using dynamic mechanical analysis (DMA) performed on a DMA 1 Instrument (Mettler-Toledo). The instrument performs DMA calculations based on the force and displacement measurements to derive the viscoelastic material parameters. The tests were carried out at 25 °C using compression platens. The EGs were cylindrical in geometry with diameters of 9 mm and a

height of 5 mm. Strain sweeps between 0.1 % strain and 6 % strain were performed at 1 Hz. Concretely, the samples are forced to undergo an oscillatory deformation in compression of 5, 10, 20, 50, 75, 100, 200, 300  $\mu\text{m}$  for 2 min at each deformation and their storage modulus ( $G'$ ) and loss modulus ( $G''$ ) obtained from the force required to produce that deformation and the geometry of the sample are recorded. Frequency sweeps from 0.1 Hz to 50 Hz were performed at strain level of 0.4 %, in the linear viscoelastic region.

## 2.11. Thermogravimetric analysis (TGA)

The thermal stability of the EGs and PFO\_CPNS@EGs was investigated in the 25–500 °C temperature range by thermogravimetric analysis (TGA) and differential thermogravimetric analysis (DTG) using a TGA/DSC 3+ (Mettler Toledo) apparatus operating under  $\text{N}_2$  atmosphere at a heating rate of 10 °C  $\text{min}^{-1}$ . Mass change was recorded as a function of temperature. The weight samples range was  $17 \pm 3$  mg.

## 2.12. Swelling characterization

Swelling measurements of the EGs were conducted with or without the inclusion of CPNs. Freshly prepared eutectogels, weighing approximately 1 g, were immersed in an excess of Milli-Q water at room temperature. The initial weight of each sample was recorded, and subsequent measurements were taken at regular intervals as the eutectogels absorbed water. The degree of swelling ( $SW$ ) was calculated using the following equation:

$$SW = \frac{W_t - W_0}{W_0} \quad (4)$$

where  $W_t$  denotes the weight of the eutectogel at time  $t$ , and  $W_0$  represents the initial weight of the freshly prepared eutectogel.

## 3. Results and discussion

### 3.1. Characterization of fluorescent CPNs in DES

At present there are very few works in which DES have been combined with fluorescent nanoparticles and in most of them DES has been used as a vehicle for their synthesis, rather than as a medium to dissolve them [32]. Therefore, before preparing the nanocomposite eutectogels we explored the behavior of the different nanoparticles solubilized in  $\text{ChCl}:\text{EtG}$  DES (1:2 M ratio). Concretely, we studied the fluorescent properties of the new solutions, comparing the results with those found in Milli-Q water and/or organic solvents.

CPNs of the different conjugated polymers, PFO, F8BT and MEHPPV were prepared as is described in Material and Methods and stocked in Milli-Q water (5 mg/mL) until used. The stock solutions were stable for months, especially when stored in the dark at 4 °C and an inert atmosphere was not required. These specific polymers were selected for their distinct emission properties across different spectral regions, facilitating the obtention of fluorescent eutectogels with varied emission bands, from 430 to around 650 nm. The size of the CPNs was determined by DLS showing diameters of 77 nm for PFO\_CPNS, 86 nm for F8BT\_CPNS and 93 nm for MEHPPV\_CPNS. From ZP analysis, CPNs showed a negative surface charge between  $-62$  and  $-29$  mV, consequence of the anionic charge of SDS, which guarantees appropriate suspension stability (Table S1).

For the study of the fluorescent properties of PFO, F8BT and MEHPPV\_CPNS, 1  $\mu\text{L}/\text{mL}$  solutions in Milli-Q water, chloroform and  $\text{ChCl}:\text{EtG}$  DES were prepared from the respective stock solutions (5 mg/mL) and their fluorescence emission spectra were recorded after excitation at 396 nm, 466 nm and 495 nm, respectively, taking into account the excitation spectra shown in Fig. S1. It is important to note that organic solvents like chloroform dissolve the conjugated polymers,

causing the nanoparticles to disintegrate. As a result, the emission spectrum observed in these solvents reflects the characteristics of the free polymer rather than the intact nanoparticles.

For PFO\_CPNS, Fig. 1a shows that the shape of the emission spectrum was similar in both water and DES, but differs significantly from the spectrum observed in chloroform. This result can be attributed to the distinct phases that PFO can adopt due to its molecular structure. As previously reported, PFO can exist in a disordered “glassy” phase or a more crystalline  $\beta$ -phase, each characterized by distinctive emission spectra and varying angles between adjacent fluorene units. In good solvents like chloroform, PFO adopts the “glassy” phase, where these angles are random. Conversely, in the  $\beta$ -phase, the fluorene units align at a fixed angle of  $180^\circ$ , resulting in a well-defined planar chain conformation that extends the conjugation length, leading to red-shifted emission [33]. This  $\beta$ -phase is adopted by PFO when the polymer is in confined media, such as a nanoparticle, and it is characterized by three distinct peaks around 438, 465, and 501 nm in the emission spectrum [34–36]. The presence of these peaks in the fluorescence spectrum in both Milli-Q water and DES (Fig. 1a) suggests that the nanoparticles remain within the DES. If the nanostructures were disrupted, the polymer would gain more degrees of freedom, transitioning to the “glassy” phase, and the emission spectrum would resemble that seen in chloroform.

A similar conclusion can be drawn when comparing the excitation spectra of the PFO\_CPNS in the three media (Fig. S1). The peak at 436 nm is a distinctive feature of the  $\beta$ -phase and its intensity was much higher in water and DES than in chloroform, confirming that in the latter medium this phase is a minority one.

Fig. 1b shows the fluorescence emission spectra of F8BT\_CPNS in DES, water and chloroform upon excitation at 466 nm. The recorded spectra are quite similar in the three media, although slightly wider in chloroform, and similar to those reported in the bibliography [37]. Unlike PFO, F8BT does not adopt any distinct phase when confined, so the shape of its spectrum remains consistent whether free or in nanoparticle form.

For MEHPPV\_CPNS, the emission profiles were similar in Milli-Q water and DES (Fig. 1c). Both the position and the maximum emission at 596 nm coincide with those described for these nanoparticles in the literature, suggesting that, as with PFO\_CPNS and F8BT\_CPNS, the integrity of the MEHPPV\_CPNS is maintained when incorporated in DES [25]. This hypothesis is supported by the fact that the spectrum obtained in chloroform shows its emission maximum at 559 nm, coinciding with that expected for the free polymer dissolved in a good organic solvent. The spectral shift observed in the CPNS compared to the polymer in solution has been attributed to the increased overlap of  $\pi$ -orbitals as the polymers aggregate within the nanoparticles. This aggregation leads to the delocalization of  $\pi$ -electrons across multiple chains resulting in a bathochromic shift [25].

Time-resolved fluorescence spectroscopy was employed to measure the fluorescence decay of the three nanoparticles in Milli-Q water and DES. The fluorescence data were analyzed using a three-exponential

decay model, and the mean fluorescence lifetime  $\langle \tau \rangle$  was derived from this fit using Equation (1), as shown in Fig. S2 and Table 1. The three CPNS showed sub-nanoseconds lifetimes with similar values in both Milli-Q-water and DES, with the F8BT\_CPNS showing the longest lifetime, as already reported in a recent work of the group, when dissolved in buffer [34].

### 3.2. Characterization of EGs and fluorescent nanocomposite EGs

EGs, in the absence of fluorescent CPNS, were synthesized by light-induced radical polymerization as described in Materials and Methods. Their shape depends on the container in which they are obtained and their final size on the volume of the starting reactants, although they can be easily cut into smaller pieces once fabricated to meet specific needs. In this work EGs were obtained in cylindrical form and in most cases, they were  $\sim 0.8$  cm in diameter and 1.7 cm in length so that they could be introduced into fluorescence cuvettes. They were easy to handle and exhibited elastic rubber properties, returning to their original dimensions after being mechanically deformed (Fig. S3). Moreover, these materials were transparent and stable, without weight loss or modification of their initial shape, even after being stored in closed vials at room temperature during 3 months (Fig. S3, Fig. 2a). This result confirms that DES is an effective solvent for the HEMA monomer and the cross-linked chains formed after its polymerization, without leading to the creation of heterogeneous microstructures, which occurred when water was used as the solvent [27].

To get more insight into the mechanical behaviour and strength of these materials and to confirm their gel nature and elastic properties, we performed oscillatory rheology measurements, namely strain- and frequency sweeps of the EGs. All the measurements were carried out at  $25^\circ\text{C}$ , as is described in Materials and Methods, and the obtained results are displayed in Figs. S4a and S4b. From these plots we can observe that the storage modulus  $G'$ , which reflects the elasticity of the material is much higher than the viscous component  $G''$  over the whole tested range of oscillation strain and angular frequency, which is the condition of the gel state. At low oscillation strain  $G'$  values were  $\sim 0.22$  MPa and the ratio of  $G'$  to  $G''$  ( $\tan \delta$ ) was  $\sim 0.1$ , values in the same range as those obtained for other eutectogels [38], indicating a strong elastic behaviour

**Table 1**

Average fluorescence lifetimes ( $\langle \tau \rangle$ ) of PFO\_CPNS, F8BT\_CPNS, and MEHPPV\_CPNS in Milli-Q water, DES and incorporated in EGs.

Sample	$\lambda_{ex}/\lambda_{em}$ (nm)	$\langle \tau \rangle$ /ns		
		Milli-Q water	DES	EG
PFO_CPNS	373/465	$0.131 \pm 0.008$	$0.159 \pm 0.005$	$0.32 \pm 0.04$
F8BT_CPNS	453/537	$0.45 \pm 0.03$	$0.59 \pm 0.04$	$0.79 \pm 0.02$
MEHPPV_CPNS	514/590	$0.122 \pm 0.013$	$0.110 \pm 0.003$	$0.277 \pm 0.011$

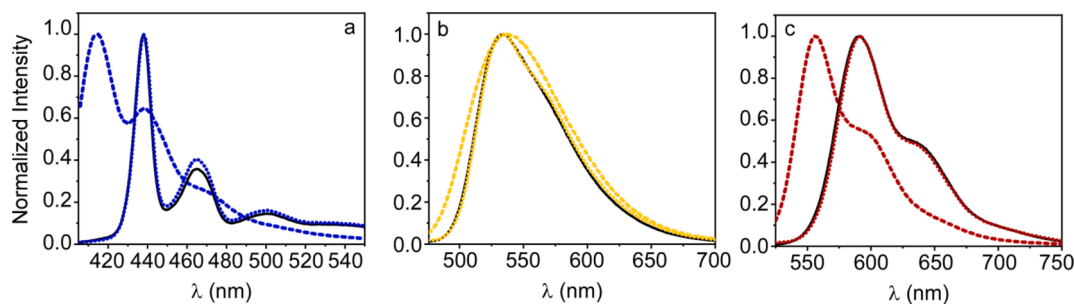


**Fig. 1.** Normalized fluorescence emission spectrum of PFO\_CPNS (a), F8BT\_CPNS (b), and MEHPPV\_CPNS (c) in Milli-Q water (black solid line), chloroform (dashed line) and ChCl:EtG DES (dotted line).

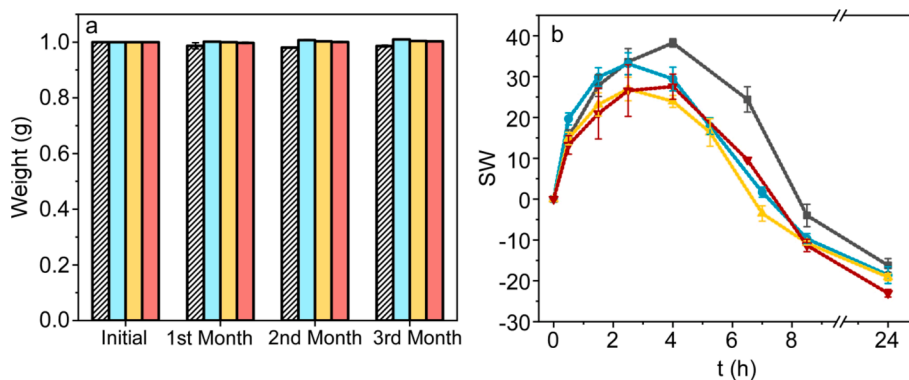


**Fig. 2.** Evolution of the eutectogel weight over time after being stored at room temperature during three months. The striped bars represent the EG in the absence of CPNs, while the blue, yellow and red bars correspond to PFO\_CPNS@EG, F8BT\_CPNS@EG and MEHPPV\_CPNS@EG, respectively (a). Swelling behavior of EGs in absence (black) and presence of PFO\_CPNS (blue), F8BT\_CPNS (yellow) and MEHPPV\_CPNS (red) immersed in water excess (b). Error bars correspond to three independent measurements.

of the material in this region, as shown previously in the digital images in Fig. S3. The fact that  $G'$  values are very weakly frequency dependent (only a slight increase was observed above 1 Hz) is evidence that the EGs show a good tolerance to the applied strain rate of deformation. In contrast  $G''$  values increased proportionally to the sweep frequency, suggesting the existence of non-covalent interactions in the internal network of the EG [39].

The stability of the eutectogel was also studied by TGA. As shown in Fig. S4c, the TGA and DTG curves depict three distinct stages of weight loss, as seen by significant peaks on the DTG curve. The TGA curve shows a high weight retention rate of 95 % at 100 °C. The first step of mass loss, between 100 and 250 °C could be attributed to the vaporization of ethylene glycol [40]. The breakage of the ester bonds in the polymeric structure (HEMA-EGDMA) as well as the vaporization of ChCl would be mainly responsible for the 2nd step of mass-loss starting from 250 °C [40,41]. Finally, the third decomposition peak, observed in the 350–470 °C range, may correspond to the complete decomposition of the polymeric structure [41].

The swelling behavior of EGs was analyzed using Milli-Q water as solvent instead of DES to assess the ability of this material to absorb and retain aqueous solutions within their network structure. This test was performed with the aim of finding out to what extent EGs can be used for applications in aqueous media, such as drug delivery or biosensing. For this purpose, a piece of eutectogel of approximately 1 g was immersed in 50 mL of Milli-Q water, and its mass was measured as a function of time. The results, expressed as degree of swelling (Equation (4)), showed that

EGs are able to absorb water increasing their mass during the first 4 h, until reaching a maximum value. However, if the material remains submerged for a longer time, a loss of mass is observed, even reaching values lower than the starting value, which suggests that after a certain time the DES begins to be exchanged for water molecules (Fig. 2b, black squares). This conclusion was supported by the fact that the immersed gel piece became increasingly whitish after a few hours, confirming what was observed in previous work where HEMA hydrogels showed an opaque appearance [27].

For the incorporation of PFO, F8BT, and MEHPPV CPNs within the EGs to obtain fluorescent nanocomposite EGs, each of these nanoparticles was mixed with the precursor, crosslinker, and photoinitiator agent using DES as solvent. The irradiation of the mixture resulted in coloured materials named PFO\_CPNS@EG, F8BT\_CPNS@EG, and MEHPPV\_CPNS@EG that retained a similar appearance to the starting eutectogel, but when placed under the UV lamp showed blue, yellow and red fluorescence, respectively, homogeneously distributed throughout the material (Fig. 3). In addition, both the shape and weight were preserved for months at room temperature when stored in closed vials, suggesting that there was no degradation or volatilization of any component during this period, unlike in the case of hydrogels (Fig. 2a).

The incorporation of CPNs in the eutectogel practically did not modify its rheological properties (Fig. S4a and S4b) and only a slight increase in the  $G'$  and  $G''$  moduli was observed in the frequency sweep, suggesting that CPNs are probably interacting with the polymeric network but that their concentration is too low to produce a more

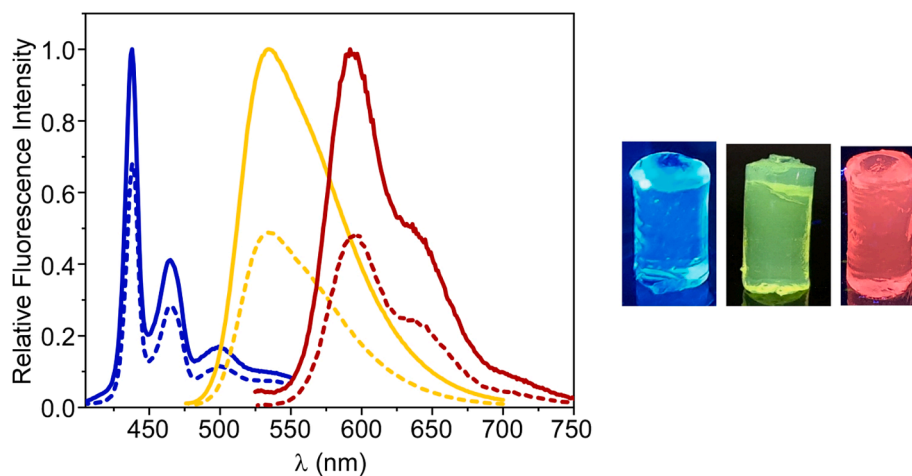


**Fig. 3.** Fluorescence emission spectrum of PFO\_CPNS@EG (blue solid line), F8BT\_CPNS@EG (yellow solid line), and MEHPPV\_CPNS@EG (red solid line) compared with those obtained for the CPNs in DES (dashed lines). right: Digital image of nanocomposite eutectogels taken under irradiation with UV light (365 nm).

noticeable change in these properties. This hypothesis is supported by the analysis of the thermal stability of the material (Fig. S4c) where it can be seen that both the TGA and DTG curves are hardly altered by the presence of the nanoparticles.

These nanocomposite EGs were introduced into a fluorescence cuvette and their emission spectra were recorded. As can be seen in Fig. 3, the fluorescence spectra were similar to those obtained in DES, although in all cases the fluorescence intensity was higher. This result indicates that the nanoparticles retain their integrity within the eutectogel, as the shape of the spectrum does not change, and also suggests further homogenization of the nanoparticles in this material and/or an increase in their fluorescence quantum yield.

The swelling behavior of fluorescent EGs was explored and compared with that observed for EGs in absence of CPNs. The results show a similar pattern of behavior, although in the case of the nanocomposites the maximum swelling was slightly lower and occurred after 2.5 h of immersion in excess water, again suggesting that the CPNs are interacting with the polymeric network (Fig. 2b). As with the eutectogel without CPNs, the DES progressively came out of the fluorescent material; however, no loss of nanoparticles was observed, since the water outside the EG showed no fluorescence signal. The retention of the CPNs inside the material was also confirmed after the analysis of the eutectogel washing residues, as shown in Fig. S5. PFO\_CPNs@EG, F8BT\_CPNs@EG, and MEHPPV\_CPNs@EG were immersed in 50 mL of Milli-Q water for 48 h. After this period, wash waters were collected and concentrated by evaporating the solvent to ensure the reliability of the results. No fluorescence was detected in this sample after resuspension in 2 mL of Milli-Q water, confirming that the nanoparticles are securely anchored to the polymeric network.

Fluorescence decays of PFO\_CPNs@EG, F8BT\_CPNs@EG and MEHPPV\_CPNs@EG were recorded and compared to those of CPNs in DES and Milli-Q water. The results show that in all three cases  $\langle \tau \rangle$  was higher than that determined for free nanoparticles in solution, although it remains within the sub-nanosecond range (Table 1, Fig. S2). This slight increase in the lifetime of the CPNs was already observed when

PFO\_CPNs were embedded in a hydrogel [34].

The thermal stability of the freshly prepared fluorescent EGs was also explored by recording the spectra at different temperatures from 20 to 60 °C (Fig. 4a-c). The results show that the temperature increase practically affects neither the fluorescence intensity nor the shape of the spectra and only a very slight decrease of the signal was observed in F8BT\_CPN@EG. This result could be attributed to the fact that, although the probability of non-radiative transitions increases with temperature as molecular collisions increase, this phenomenon would be much less likely in an eutectogel than in a solution, due to the immobilization of the CPNs in the material.

The effect of storage time on the fluorescent EGs was also explored. To this end, PFO\_CPNs@EG, F8BT\_CPNs@EG, and MEHPPV\_CPNs@EG freshly prepared were stored at 4 °C and their emission spectra were recorded on different days. Fig. 4d-f shows the fluorescence intensity of these eutectogels measured on the first day of preparation and for one month. The results show that the three EGs were stable for the first 10 days, but after 20 days, only PFO\_CPNs@EG and F8BT\_CPNs@EG maintained a fluorescence close to the initial one, while the MEHPPV\_CPNs@EG decreased its fluorescence signal, probably due to the higher tendency of these nanoparticles to aggregate (lower Z potential).

### 3.3. Fluorescent nanocomposite EGs as sensing platforms

Potential applications of fluorescent eutectogels include their use for the detection of compounds of interest by inducing changes in their luminescent properties. Such changes can involve either an enhancement or reduction in fluorescence intensity or alterations in their emission spectra. The advantage, compared to hydrogels, is that they can detect analytes whether they are present in solution or in air due to the non-volatility of DES. In this work we have evaluated the suitability of these materials for use in aqueous media, in particular, their ability to detect *p*-nitrophenol (PNP). This compound is widely used in the manufacture of various industrial products such as paints, plasticizers,

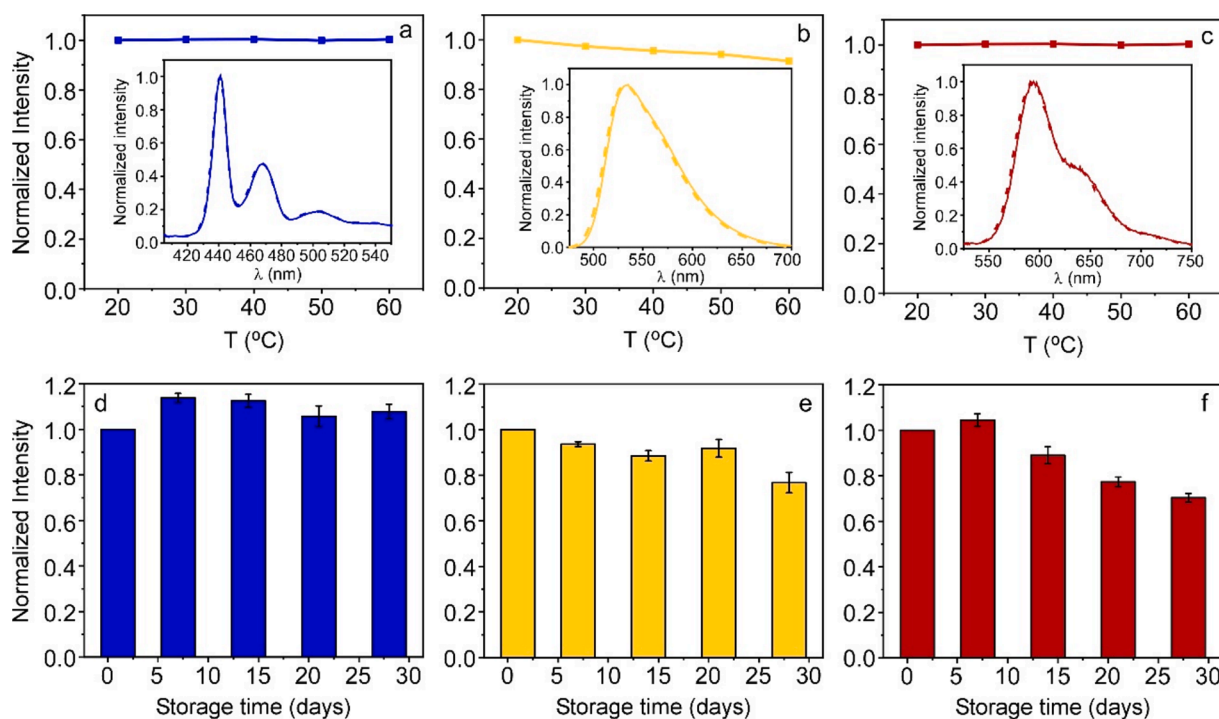


Fig. 4. Effect of temperature and storage time on the stability of PFO\_CPNs@EG (a, d), F8BT\_CPNs@EG (b, e) and MEHPPV\_CPNs@EG (c, f) measured at the fluorescence intensity maximum. Insets: Normalized fluorescence emission spectra at 20 °C (solid line) and 60 °C (dashed line) (a, b, c). Error bars correspond to three independent measurements.

pesticides, pharmaceuticals, explosives and textiles, and its exploitation creates serious environmental problems [42]. PNP is also the hydrolysis end-product of certain hydrolases enzymes such as  $\alpha$ -glucosidase, lipase or alkaline phosphatase (ALP). In addition, it is an electron acceptor that absorbs at 400 nm in its anionic form, and has been previously described to be able to quench the fluorescence of polyfluorenes and carbon dots [43,44]. The availability of fluorescent materials susceptible to be quenched by this compound offers the possibility of developing sensing platforms to detect its presence in natural water systems as well for investigating the activity of various hydrolase enzymes, measuring their concentrations, or identifying their inhibitors [45,46].

With this in mind, we study whether the fluorescent eutectogels developed in this work showed any response to the presence of PNP. For this purpose and as a first step, we explored the effect of this compound on the fluorescence intensity of PFO\_CPNs, F8BT\_CPNs, and MEHPPV\_CPNs in TRIS buffer solution, selecting the excitation/emission conditions in which this effect was most noticeable. Fig. S6 shows that at a specific concentration of PNP, the fluorescence of all three CPNs is quenched, with the most significant decrease occurring at an excitation wavelength near 400 nm. The fact that the absorption maximum of the anionic PNP is around this wavelength suggests that primary inner filter effects (IFE) could be one of the responsible mechanisms for such fluorescence reduction, since in the presence of PNP the excitation light would get attenuated before reaching the fluorophores.

To verify the fluorescence response of the nanoparticles towards PNP, three similar solutions of PFO\_CPNs, F8BT\_CPNs, and MEHPPV\_CPNs in TRIS buffer were prepared, and increasing concentrations of PNP up to 20  $\mu\text{M}$ , were added. The results obtained are displayed in Fig. 5a in the form of a Stern-Volmer plot. The fluorescence intensity gradually decreased with the addition of PNP and the quenching effect was very evident. Experimental results indicate that all three nanoparticles could be capable of detecting PNP, with K values (equation (2) of  $3.21 \pm 0.07 \times 10^4 \text{ M}^{-1}$  (PFO\_CPNs),  $2.29 \pm 0.04 \times 10^4$  (F8BT\_CPNs) and  $2.33 \pm 0.05 \times 10^4 \text{ M}^{-1}$  (MEHPPV\_CPNs). The higher sensitivity of the blue nanoparticles could be due to the fact that the absorption spectrum of PNP overlaps with the emission spectrum of PFO\_CPNs (especially with the peak of maximum emission), but not with those of F8BT and MEHPPV nanoparticles, so that in addition to primary IFEs, secondary IFEs and other possible mechanisms such energy transfer could be involved in the attenuation of the fluorescence, as has been recently reported for other PNP fluorescent sensors [44,46]. The fact that both CPNs and PNPs are negatively charged suggests that a complex is unlikely to form between the two species, thereby eliminating static quenching and charge transference as the cause of fluorescence loss in all three cases. Furthermore, the average lifetime of the three nanoparticles was found to be similar in buffer, in presence and absence of PNP (Table S2), although the fluorescence signal decreased, which probably also excludes energy transfer as the dominant

mechanism for PNP quenching.

To assess the role of IFE in fluorescence quenching, fluorescence intensities in absence and presence of 20  $\mu\text{M}$  PNP were corrected for the three CPNs using equation (3). For this purpose, we measured the absorbance of the samples at the excitation and emission wavelengths of the fluorophores. These measurements allowed to calculate the corrected fluorescence intensity, accounting for any reabsorption and attenuation of the emitted light. After correction, the  $I_0/I$  ratio at 20  $\mu\text{M}$  PNP was 1.33; 1.06 and 1.06 for PFO\_CPNs, F8BT\_CPNs, and MEHPPV\_CPNs, respectively. It is thus evident that the IFE plays an important role in the fluorescence quenching, being probably the only mechanism causing the observed fluorescence reduction in F8BT\_CPNs and MEHPPV\_CPNs. For PFO\_CPNs, although IFE is the major factor contributing to quenching, other mechanisms, probably energy transfer, due to spectral overlap with PNP absorption, could also play a role. However, this contribution is minor and would practically not affect the lifetime measurements since it adds minimally to the overall quenching effect.

Quenching effects were also observed when PNP was directly added to PFO\_CPNs@EG, F8BT\_CPNs@EG and MEHPPV\_CPNs@EG. To perform these experiments, the fluorescent eutectogels were introduced into cuvettes and their initial fluorescence spectra were measured, as is described in section 2.9. Then, 1 mL of a PNP solution (20, 50 or 100  $\mu\text{M}$  in TRIS buffer) was added to each cuvette and, after 20 min incubation to allow diffusion and homogenization of the sample, their fluorescence spectra were recorded. Fig. 5b shows the initial emission spectra of the three fluorescent eutectogels compared to those obtained after the addition of 100  $\mu\text{M}$  PNP. As can be seen, PFO\_CPNs@EG exhibited the highest sensitivity to PNP, with its fluorescence spectrum showing the greatest reduction in signal, as was the case in solution. This same behaviour was observed with the other two PNP concentrations studied. Furthermore, as in solution, the response was linear, with gradual decrease in fluorescence intensity as the PNP concentration increased (Fig. S7).

From these experiments we designated PFO\_CPN@EG as the most suitable material to build our biosensor platform. As a proof of concept, we selected the enzyme ALP, capable of hydrolyzing the substrate *p*-nitrophenyl phosphate (PNPP) into PNP. The activity of this enzyme has been utilized in various sensor design applications, either for the direct detection of analytes (enzyme substrates) or for the indirect measurement of organic and inorganic substances, such as phosphate, heavy metals, organophosphorus pesticides, and biologically active metabolites, which function as enzyme inhibitors [43,47,48]. Our objective was to demonstrate that the enzyme was able to maintain its activity inside the material, and that this could be monitored from the decrease in the fluorescence intensity induced by the production of PNP.

To this end, ALP was immobilized in the eutectogel simultaneously to PFO\_CPNs obtaining fluorescent eutectozymes, as described in

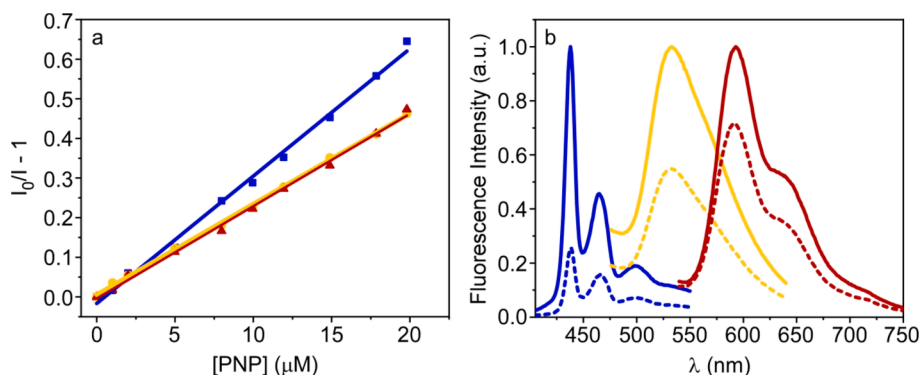


Fig. 5. Stern-Volmer plot for quenching of PFO\_CPNs (blue line), F8BT\_CPNs (yellow line), and MEHPPV\_CPNs (red line) in TRIS buffer at increasing concentrations of PNP up to 20  $\mu\text{M}$  (a). Fluorescence emission spectra of PFO\_CPNs@EG (blue solid line), F8BT\_CPNs@EG (yellow solid line) and MEHPPV\_CPNs@EG (red solid line) compared with those obtained in the presence of 100  $\mu\text{M}$  PNP solution (dashed blue, yellow and red lines respectively) (b).



**Materials and Methods.** The resulting materials, hereinafter referred to as ALP@PFO@EG, were deposited in cuvettes and their fluorescence signal was measured, proving that their emission spectrum was not affected by containing the enzyme. Moreover, in successive preparations of eutectozymes, the fluorescence intensity was practically similar, demonstrating reproducibility in the nanocomposite fabrication (Fig. S8).

The catalytic activity of ALP@PFO@EG, was tested by addition of solutions of PNPP (50 and 100  $\mu\text{M}$ ) to the prepared eutectozyms. Fig. 6 shows the initial fluorescence spectrum of ALP@PFO@EG and those obtained after adding either 1 mL of buffer or 1 mL of buffer containing PNPP, recorded 60 min after addition. This incubation time was selected according to a previous experiment in which it was shown that practically the fluorescence signal stabilized after this period of time (Fig. S9). The results showed a decrease in the fluorescence of the EGs containing PNPP, the higher the concentration of PNPP the greater the decrease. This result demonstrates that the enzyme retains its activity within the nanocomposite and that this can be monitored by tracking variations in the fluorescence signal. It highlights the potential of these materials to serve as fluorescent biosensors for detecting enzyme inhibitors that are relevant in environmental and biological contexts. Additionally, these findings mark one of the earliest demonstrations of an enzyme functioning within an eutectogel.

#### 4. Conclusions

Fluorescent nanoparticles based on conjugated polymers with emission in the blue (PFO\_CPNS), yellow (F8BT\_CPNS) and red (MEHPPV\_CPNS) spectral regions have been effectively solubilized in DES composed of choline chloride and ethylene glycol while retaining their fluorescent properties. This has enabled the development of novel fluorescent nanocomposite eutectozyms through a straightforward synthesis method involving UV-initiated radical polymerization within the DES, where the nanoparticles, HEMA monomer, EGDMA crosslinker and a photoinitiator were successfully combined. These new materials are rigid, flexible, easy-to-handle and transparent and display fluorescence emission spectra similar to those of the original nanoparticles but with slightly longer fluorescent lifetimes. In addition, they are stable to temperature changes and can be stored for several weeks without altering their weight and fluorescent properties, especially the PFO and F8BT formulations. EGs also exhibited swelling behaviour, allowing water molecules to be absorbed, which could make them suitable as potential sensor systems, not only in dry, but also in aqueous environments. This capability was demonstrated by adding the compound PNP, which reduced the fluorescence of EGs, with the PFO\_CPNS@EG showing the highest sensitivity to its presence, the inner filter effect being mainly responsible for this effect. This result led to the development of a prototype of fluorescent biosensor for detecting hydrolase activity, achieved by co-immobilizing the enzyme ALP together with PFO\_CPNS, resulting in fluorescent eutectozyms that enhance the functionality of the material. This finding represents one of the first instances of an enzyme successfully operating within an eutectogel.

These results suggest that fluorescent nanocomposite EGs, such as those developed in this work, both in the absence and presence of enzymes, are very promising for applications in advanced materials, capable of operating in different environments. This encourages further research and development in this innovative field to exploit their full potential in various technological and biomedical applications.

#### CRediT authorship contribution statement

**Yolanda Alacid:** Writing – original draft, Methodology, Investigation, Formal analysis, Data curation. **Raúl Martínez-Baquero:** Visualization, Methodology, Investigation, Data curation. **Rocío Esquembre:** Writing – original draft, Validation, Methodology, Investigation, Formal analysis. **Francisco Montilla:** Resources, Project administration,

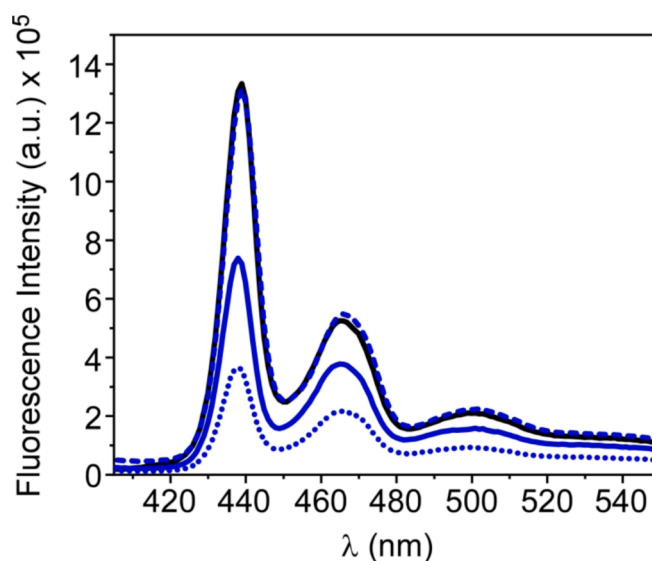


Fig. 6. Fluorescence emission spectra of ALP@PFO@EG in the absence (black line) and presence of TRIS buffer (blue dashed line), 50  $\mu\text{M}$  (blue solid line) and 100  $\mu\text{M}$  (blue dotted line) of PNPP solution.

**Methodology, Funding acquisition. María José Martínez-Tomé:** Visualization, Supervision, Project administration, Methodology, Investigation, Data curation. **C. Reyes Mateo:** Writing – review & editing, Writing – original draft, Visualization, Supervision, Resources, Project administration, Funding acquisition, Conceptualization.

#### Funding

This work was funded by the Spanish MICIU/AEI/10.13039/501100011033 (grant PID2022-138507OB-I00) and the Conselleria de Innovación, Universidades, Ciencia y Sociedad Digital (grants CIAICO/2022/131 and MFA/2022/058), and by the Spanish MCIN (grant TED2021-129894B-I00). DLS and Fluorescence lifetime spectrometer equipment acquisition funded by Generalitat Valenciana –Conselleria d’Educació Investigació Cultura i Esport and EUFEDER “Una forma de hacer Europa” (GVA-IDIFEDER/2018/020 and GVAIDIFEDER/2021/036).

#### Declaration of competing interest

The authors declare that they have no known competing financial interests or personal relationships that could have appeared to influence the work reported in this paper.

#### Acknowledgements

We thank Dr Ion Such for his kind help in the rheological and thermal characterisation of the eutectozyms.

#### Appendix A. Supplementary data

Supplementary data to this article can be found online at <https://doi.org/10.1016/j.molliq.2025.127123>.

#### Data availability

Data will be made available on request.

## References

- [1] M. Chelu, A.M. Musuc, Polymer gels: classification and recent developments in biomedical applications, *Gels* 9 (2023) 161, <https://doi.org/10.3390/GELS9020161>.
- [2] P.C. Marr, A.C. Marr, Ionic liquid gel materials: applications in green and sustainable chemistry, *Green Chem.* 18 (2015) 105–128, <https://doi.org/10.1039/C5GC02277K>.
- [3] Y. Nahar, S.C. Thickett, Greener, faster, stronger: the benefits of deep eutectic solvents in polymer and materials science, *Polymers* 13 (2021) 447, <https://doi.org/10.3390/POLYM13030447>.
- [4] J. Ruiz-Olles, P. Slavik, N.K. Whitelaw, D.K. Smith, Self-assembled gels formed in deep eutectic solvents: supramolecular eutectogels with high ionic conductivity, *Angew. Chem. Int. Ed.* 58 (2019) 4173–4178, <https://doi.org/10.1002/ANIE.201810600>.
- [5] E.L. Smith, A.P. Abbott, K.S. Ryder, Deep eutectic solvents (DESS) and their applications, *Chem. Rev.* 114 (2014) 11060–11082, <https://doi.org/10.1021/CR300162P>.
- [6] T. Swebocki, A. Barras, A. Abderrahmani, K. Haddadi, R. Boukherroub, Deep eutectic solvents comprising organic acids and their application in (bio)medicine, *Int. J. Mol. Sci.* 24 (2023) 8492, <https://doi.org/10.3390/IJMS24108492>.
- [7] P. De Moraes, F. Gonçalves, J.A.P. Coutinho, S.P.M. Ventura, Ecotoxicity of cholinium-based deep eutectic solvents, *ACS Sustain. Chem. Eng.* 3 (2015) 3398–3404, <https://doi.org/10.1021/ACSSUSCHEMENG.5B01124>.
- [8] L. Meredith, A. Elbourne, T.L. Greaves, G. Bryant, S.J. Bryant, Physico-chemical characterisation of glycerol- and ethylene glycol-based deep eutectic solvents, *J. Mol. Liq.* 394 (2024) 123777, <https://doi.org/10.1016/J.MOLLIQ.2023.123777>.
- [9] P.A. Mercadal, A. González, A. Beloqui, L.C. Tomé, D. Mecerreyes, M. Calderón, M. L. Picchio, Eutectogels: The Multifaceted Soft Ionic Materials of Tomorrow, *JACS Au* 4 (2024) 3744–3758, <https://doi.org/10.1021/JACS.4C00677>.
- [10] M.B. Bianchi, C. Zhang, E. Catlin, G. Sandri, M. Calderón, E. Larrañeta, R. F. Donnelly, M.L. Picchio, A.J. Paredes, Bioadhesive eutectogels supporting drug nanocrystals for long-acting delivery to mucosal tissues, *Mater. Today Bio* 17 (2022) 100471, <https://doi.org/10.1016/J.MTBIO.2022.100471>.
- [11] M. Criado-Gonzalez, N. Alegret, A.M. Fracaroli, D. Mantione, G. Guzmán-González, R. Del Olmo, K. Tashiro, L.C. Tomé, M.L. Picchio, D. Mecerreyes, Mixed conductive, injectable, and fluorescent supramolecular eutectogel composites, *Angew. Chem. Int. Ed.* 62 (2023) e202301489, <https://doi.org/10.1002/ANIE.202301489>.
- [12] J. Wang, S. Zhang, Z. Ma, L. Yan, Deep eutectic solvents eutectogels: progress and challenges, *Green Chem. Eng.* 2 (2021) 359–367, <https://doi.org/10.1016/J.GCE.2021.06.001>.
- [13] M.A. Quazi, D. Kundu, Density functional theory assessment of molecular interactions and electronic properties in lithium Bis(trifluoromethanesulfonyl) imide with inorganic and organic polymer derived eutectogel, *J. Power Sources* 597 (2024) 234129, <https://doi.org/10.1016/J.JPOWSOUR.2024.234129>.
- [14] J. G. de Araujo Lima e Souza, M.E. Di Pietro, A. Mele, Eutectic solvents and low molecular weight gelators for next-generation supramolecular eutectogels: a sustainable chemistry perspective, *RSC Sustain.* 2 (2024) 288–319. DOI: 10.1039/D3SU00264K.
- [15] Z.L. Shaw, M.N. Awad, S. Gharehgozlo, T.L. Greaves, H. Haidari, Z. Kopecki, G. Bryant, P.T. Spicer, S. Wallia, A. Elbourne, S.J. Bryant, Deep Eutectic Solvent Eutectogels for Delivery of Broad-Spectrum Antimicrobials, *ACS Appl. Biol. Mater.* 7 (2024) 1429–1434, <https://doi.org/10.1021/ACSABM.3C00971>.
- [16] Z. Asghari, H. Sereshi, S. Soltani, M. Taghizadeh, S. Karami, M. Esmaeili Bidhendi, S. Rezanian, An alginate-based eutectogel impregnated with polyvinylpyrrolidone/benzoic acid deep eutectic solvent and magnetic carboxylated multiwalled carbon nanotubes: Evaluated as sorbent in green microextraction of pesticides, *J. Chromatogr. B* 1229 (2023) 123865, <https://doi.org/10.1016/J.JCHROMB.2023.123865>.
- [17] J. Yang, Y. Feng, B. Wang, J. Miao, S. Wei, H. Li, L. Mo, Z. Qin, Tough, multifunctional, and green double-network binary solvent eutectogel with in-situ generation of lignin nanoparticles based on one-step dual phase separations for wearable flexible strain sensors, *Chem. Eng. J.* 474 (2023) 145544, <https://doi.org/10.1016/J.CEJ.2023.145544>.
- [18] C. Li, J. Liu, X. Qiu, X. Yang, X. Huang, X. Zhang, Photoswitchable and Reversible Fluorescent Eutectogels for Conformal Information Encryption, *Angew. Chem. Int. Ed.* 62 (2023) e202313971, <https://doi.org/10.1002/ANIE.202313971>.
- [19] P. Tandale, N. Choudhary, J. Singh, A. Sharma, A. Shukla, P. Sriram, U. Soni, N. Singla, R.P. Barnwal, G. Singh, I.P. Kaur, A. Sutte, Fluorescent quantum dots: An insight on synthesis and potential biological application as drug carrier in cancer, *Biochem. Biophys. Rep.* 26 (2021) 100962, <https://doi.org/10.1016/J.BBREP.2021.100962>.
- [20] X. Gao, C. Du, Z. Zhuang, W. Chen, Carbon quantum dot-based nanoprobe for metal ion detection, *J. Mater. Chem. C Mater.* 4 (2016) 6927–6945, <https://doi.org/10.1039/C6TC02055K>.
- [21] M. Bacon, S.J. Bradley, T. Nann, Graphene Quantum Dots, *Part. Part. Syst. Char.* 31 (2014) 415–428, <https://doi.org/10.1002/PPSC.201300252>.
- [22] C.A. Echeverry-Gonzalez, V.V. Kouznetsov, Carbon Dots: An Insight into Their Application in Heavy Metal Sensing, *Recent Prog. Mater.* 3 (2021) 1–17, <https://doi.org/10.21926/RPM.2102015>.
- [23] E.C. Silva, J. Pina, R.F.P. Pereira, D. Murtinho, A.J.M. Valente, A.R. Fajardo, Synthesis and characterization of fluorescent poly( $\alpha$ -cyclodextrin)/carbon quantum dots composite for efficient removal and detection of toluene and xylene from aqueous media, *Environ. Pollut.* 347 (2024) 123778, <https://doi.org/10.1016/J.ENVPOL.2024.123778>.
- [24] M. Rubio-Camacho, Y. Alacid, R. Mallavia, M.J. Martínez-Tomé, C. Reyes Mateo, Polyfluorene-Based Multicolor Fluorescent Nanoparticles Activated by Temperature for Bioimaging and Drug Delivery, *Nanomaterials* 9 (2019) 1485. DOI: 10.3390/NANO9101485.
- [25] M. Green, P. Howes, C. Berry, O. Argyros, M. Thanou, Simple conjugated polymer nanoparticles as biological labels, *Proceedings of the Royal Society A: Mathematical, Physical and Engineering Sciences* 465 (2009) 2751–2759. DOI: 10.1098/RSPA.2009.0181.
- [26] K. Kumar, M. Calderón, A. Beloqui, M.L. Picchio, Spectroscopic Eutectogels as Promising Materials in Biocatalysis, *ChemCatChem* 16 (2024) e202400204, <https://doi.org/10.1002/cctc.202400204>.
- [27] T.Y. Chen, Y.J. Jiang, H.W. Chien, Developing Transparent and Conductive PolyHEMA Gels Using Deep Eutectic Solvents, *Polymers* 15 (2023) 2605, <https://doi.org/10.3390/POLYM15122605>.
- [28] H. Qin, M.J. Panzer, Chemically Cross-Linked Poly(2-hydroxyethyl methacrylate)-Supported Deep Eutectic Solvent Gel Electrolytes for Eco-Friendly Supercapacitors, *ChemElectroChem* 4 (2017) 2556–2562, <https://doi.org/10.1002/CELC.201700586>.
- [29] J. Pecher, S. Mecking, Nanoparticles of conjugated polymers, *Chem. Rev.* 110 (2010) 6260–6279, <https://doi.org/10.1021/CR100132Y>.
- [30] A. Coutinho, M. Prieto, Ribonuclease T1 and alcohol dehydrogenase fluorescence quenching by acrylamide: A laboratory experiment for undergraduate students, *J. Chem. Educ.* 70 (1993) 425–428, <https://doi.org/10.1021/ED070P425>.
- [31] C.R. Mateo, M. Prieto, V. Micol, S. Shapiro, J. Villalán, A fluorescence study of the interaction and location of (+)-totalol, a terpenoid bioactive molecule, in model membranes, *Biochim. Biophys. Acta Biomembr.* (1509 (2000)) 167–175, [https://doi.org/10.1016/S0005-2736\(00\)00291-1](https://doi.org/10.1016/S0005-2736(00)00291-1).
- [32] R. Tabaraki, F. Nazari, Comparison of Carbon Dots Prepared in Deep Eutectic Solvent and Water/Deep Eutectic Solvent: Study of Fluorescent Detection of Fe<sup>3+</sup> and Cetirizine and their Photocatalytic Antibacterial Activity, *J. Fluoresc.* 32 (2022) 549–558, <https://doi.org/10.1007/S10895-021-02875-1>.
- [33] H.J. Eggimann, F. Le Roux, L.M. Herz, How  $\beta$ -Phase Content Moderates Chain Conjugation and Energy Transfer in Polyfluorene Films, *J. Phys. Chem. Lett.* 10 (2019) 1729–1736, <https://doi.org/10.1021/ACS.JPLETT.9B00483>.
- [34] Y. Alacid, R. Esquembre, F. Montilla, M.J. Martínez-Tomé, C.R. Mateo, Fluorescent Nanocomposite Hydrogels Based on Conjugated Polymer Nanoparticles as Platforms for Alkaline Phosphatase Detection, *Biosensors* 13 (2023) 408, <https://doi.org/10.3390/BIOS13030408>.
- [35] C. Wu, J. McNeill, Swelling-controlled polymer phase and fluorescence properties of polyfluorene nanoparticles, *Langmuir* 24 (2008) 5855–5861, <https://doi.org/10.1021/LA8000762>.
- [36] X. Zhao, R. Li, Y. Jia, Tuning the formation of  $\beta$ -phase poly(9,9-di-n-octylfluorenyl-2,7-diy) via nano-confinement and polystyrene blending for improved photocatalysis, *ChemPhysMater* 1 (2022) 219–226, <https://doi.org/10.1016/J.CHPHMA.2022.03.003>.
- [37] L. Urbano, L. Clifton, H.K. Ku, H. Kendall-Troughton, K.K.A. Vandera, B.F. E. Matarese, T. Abelha, P. Li, T. Desai, C.A. Dreiss, R.D. Barker, M.A. Green, L. A. Dailey, R.D. Harvey, Influence of the Surfactant Structure on Photoluminescent  $\pi$ -Conjugated Polymer Nanoparticles: Interfacial Properties and Protein Binding, *Langmuir* 34 (2018) 6125–6137, <https://doi.org/10.1021/ACS.LANGMUIR.8B00561>.
- [38] V. Vanoli, J. Pietrowska, G. De, A. Lima, M.E. Souza, P. Di, F. Briatico Vangosa, A. Mele, F. Castiglione, Supramolecular Hydrophobic Eutectogels Based on Menthol-Thymol as Thermo- and pH-Responsive Drug Delivery Systems, *ACS Applied Engineering Materials* 2 (2024) 388–396. DOI: 10.1021/ACSAENM.3C00697.
- [39] H. Xia, M. Ren, Y. Zou, S. Qin, C. Zeng, Novel Biocompatible Polysaccharide-Based Eutectogels with Tunable Rheological, thermal, and mechanical properties: the role of water, *Molecules* 25 (2020) 3314, <https://doi.org/10.3390/MOLECULES25153314>.
- [40] N. Delgado-Mellado, M. Larriba, P. Navarro, V. Rigual, M. Ayuso, J. García, F. Rodríguez, Thermal stability of choline chloride deep eutectic solvents by TGA/FTIR-ATR analysis, *J. Mol. Liq.* 260 (2018) 37–43, <https://doi.org/10.1016/J.MOLLIQ.2018.03.076>.
- [41] Ö. Kesmez, E. Arpaç, N. Kiraz, N.T. Selli, A. Tunali, Mechanical, anti-bacterial, and easy-to-clean properties of hybrid polymer-based composites containing modified SiO<sub>2</sub> prepared by thermal polymerization, *Chem. Pap.* 74 (2020) 3383–3398, <https://doi.org/10.1007/S11696-020-01167-5>.
- [42] Z. Xiong, H. Zhang, W. Zhang, B. Lai, G. Yao, Removal of nitrophenols and their derivatives by chemical redox: A review, *Chem. Eng. J.* 359 (2019) 13–31, <https://doi.org/10.1016/J.CEJ.2018.11.111>.
- [43] Z. Kahveci, M.J. Martínez-Tomé, R. Mallavia, C.R. Mateo, Fluorescent biosensor for phosphate determination based on immobilized polyfluorene-liposomal nanoparticles coupled with alkaline phosphatase, *ACS Appl. Mater. Interfaces* 9 (2017) 136–144, <https://doi.org/10.1021/ACSAMI.6B12434>.
- [44] K. Sasikumar, R. Rajamanikandan, H. Ju, Inner filter effect-based highly sensitive quantification of 4-nitrophenol by strong fluorescent N, S co-doped carbon dots, *Carbon Lett.* 34 (2024) 851–863, <https://doi.org/10.1007/S42823-023-00666-1>.
- [45] Y. Alacid, M.J. Martínez-Tomé, C.R. Mateo, Reusable Fluorescent Nanobiosensor Integrated in a Multiwell Plate for Screening and Quantification of Antidiabetic Drugs, *ACS Appl. Mater. Interfaces* 13 (2021) 25624–25634, <https://doi.org/10.1021/ACSAMI.1C02505>.
- [46] P. Venugopalan, N. Vidya, Microwave assisted green synthesis of carbon dots from sweet flag (*Acorus calamus*) for fluorescent sensing of 4-nitrophenol,

- J. Photochem. Photobiol. A Chem. 439 (2023) 114625, <https://doi.org/10.1016/J.JPHOTOCHEM.2023.114625>.
- [47] A. Gödel, A. Marmur, G.R. Kasaliwal, P. Pötschke, G. Heinrich, Shape-dependent localization of carbon nanotubes and carbon black in an immiscible polymer blend during melt mixing, *Macromolecules* 44 (2011) 6094–6102, <https://doi.org/10.1021/MA200793A>.
- [48] Y. Alacid, A.F. Quintero Jaime, M.J. Martínez-Tomé, C.R. Mateo, F. Montilla, Disposable Electrochemical Biosensor Based on the Inhibition of Alkaline Phosphatase Encapsulated in Acrylamide Hydrogels, *Biosensors* 12 (2022) 698, <https://doi.org/10.3390/BIOS12090698>.